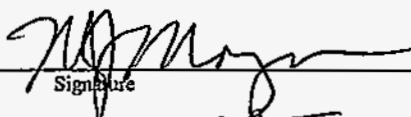
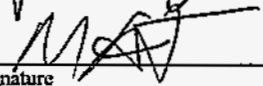


**TRITIUM AND DECAY HELIUM EFFECTS ON THE  
FRACTURE TOUGHNESS PROPERTIES OF TYPES  
316L, 304L AND 21CR-6NI-9MN STAINLESS STEELS\***

Michael J. Morgan and Michael H. Tosten  
Westinghouse Savannah River Company  
Savannah River Technology Center  
Aiken, SC 29803, USA

  
\_\_\_\_\_  
Signature Date 9/9/94

  
\_\_\_\_\_  
Signature Date 9/9/94

A paper proposed for presentation

Fifth International Conference  
on Hydrogen Effects on Material Behavior

Moran, Wyoming  
September 11-15, 1994

and for publication in the conference proceedings

---

\*This article was prepared in connection with work done under Contract No. DE-AC09-89SR18035 with the U. S. Department of Energy. By acceptance of this article, the publisher and/or recipient acknowledges the U. S. Government's right to retain a non-exclusive, royalty-free license in and to any copyright covering this article, along with the right to reproduce and to authorize others to reproduce all or part of the copyrighted article.

**MASTER**

## DISCLAIMER

This report was prepared as an account of work sponsored by an agency of the United States Government. Neither the United States Government nor any agency thereof, nor any of their employees, makes any warranty, express or implied, or assumes any legal liability or responsibility for the accuracy, completeness, or usefulness of any information, apparatus, product, or process disclosed, or represents that its use would not infringe privately owned rights. Reference herein to any specific commercial product, process, or service by trade name, trademark, manufacturer, or otherwise does not necessarily constitute or imply its endorsement, recommendation, or favoring by the United States Government or any agency thereof. The views and opinions of authors expressed herein do not necessarily state or reflect those of the United States Government or any agency thereof.

This report has been reproduced directly from the best available copy.

Available to DOE and DOE contractors from the Office of Scientific and Technical Information, P.O. Box 62, Oak Ridge, TN 37831; prices available from (615) 576-8401.

Available to the public from the National Technical Information Service, U.S. Department of Commerce, 5285 Port Royal Road, Springfield, VA 22161.

## **DISCLAIMER**

**Portions of this document may be illegible in electronic image products. Images are produced from the best available original document.**

## TRITIUM AND DECAY HELIUM EFFECTS ON THE FRACTURE TOUGHNESS

### PROPERTIES OF TYPES 316L, 304L AND 21CR-6NI-9MN STAINLESS STEELS\*

Michael J. Morgan and Michael H. Tosten

Westinghouse Savannah River Company  
Savannah River Technology Center  
Aiken, SC 29808, US

#### Abstract

J-integral fracture mechanics techniques and electron microscopy observations were used to investigate the effects of tritium and its radioactive decay product,  $^3\text{He}$ , on Types 316L, 304L and 21Cr-6Ni-9Mn stainless steels. Tritium-exposed-and-aged steels had lower fracture-toughness values and shallower sloped crack-growth-resistance curves than unexposed steels. Both fracture-toughness parameters decreased with increasing concentrations of  $^3\text{He}$ . The fracture-toughness reductions were accompanied by a change in fracture mode from microvoid-nucleation-and-growth processes in control samples to grain-and-twin-boundary fracture in tritium-charged-and-aged samples. Type 316L stainless steel had the highest fracture-toughness values and Type 21Cr-6Ni-9Mn had the lowest. Samples containing  $^3\text{He}$  but degassed of tritium had fracture toughness properties that were similar to uncharged samples. The results indicate that helium bubbles enhance the embrittlement effects of hydrogen by affecting the deformation properties and by increasing localized hydrogen concentrations through trapping effects.

\* This article was prepared in connection with work done under Contract No. DE-AC09-89SR18035 with the U. S. Department of Energy.

## Introduction

Austenitic stainless steels exposed to tritium are embrittled more than those exposed to hydrogen or deuterium because of the effects of the radioactive decay product of tritium, helium-3 ( $^3\text{He}$ ). Helium is virtually insoluble in the lattice and when it is born in the metal from tritium decay it is trapped quickly and precipitates out as a bubble on vacancy clusters, microstructural defects, or other helium atoms. Helium-bubble pinning of dislocations causes large increases in the flow stress and changes the deformation behavior to one dominated by deformation twinning (1,2). Moreover, the presence of helium bubbles on grain boundaries tend to trap hydrogen and help to promote intergranular fracture (3-6).

The degree to which austenitic stainless steels are embrittled by hydrogen isotopes is greatly affected by material composition. For example, alloying elements which decrease the stacking fault energy—such as nitrogen and manganese—increase the steel's sensitivity to hydrogen embrittlement and alloying elements which increase the stacking fault energy—such as nickel—decrease the hydrogen embrittlement sensitivity (3). J-integral fracture mechanics techniques are useful for quantifying these effects. Measurements of  $J_{IC}$  and the J-R curve can be used to establish the lifetimes of structural materials for tritium applications in which stress conditions are known and for which inspection flaw size limits can be established.

In this study, J-integral fracture mechanics and electron microscopy techniques were used to investigate the combined effects of tritium and  $^3\text{He}$  on Types 304L, 316L, and 21-6-9 stainless steels. The purposes of the study were to: (1) Quantify the fracture toughness reductions as a function of  $^3\text{He}$  content; (2) Characterize the decay  $^3\text{He}$  bubble microstructures; and, (3) Relate the effects of hydrogen and helium to recent brittle fracture models of austenitic steels.

## Experimental Procedure

Arc-shaped fracture-mechanics specimens were fabricated from high-energy-rate-forged (HERF) forward-extruded cylinders. The samples had an inside radius of 6.35 mm, an outside radius of 12.7 mm, a thickness of 3.81 mm, and an initial fatigue-crack length to width ratio between 0.4 and 0.7. The samples were machined such that the crack plane was normal to the forging's circumferential direction and the direction of crack propagation was in the radial direction. The compositions and mechanical properties of the steels are given in Table I.

The specimens were thermally charged at 423 K with a tritium partial pressure of 29 MPa for six to nine months. The samples were then aged at 273 K for selected times to allow for decay to  $^3\text{He}$  while minimizing offgassing losses of tritium. The surface concentrations of tritium and  $^3\text{He}$  were calculated based on diffusivity and solubility data and a finite-difference computer code (3). The calculated values listed in Table II were checked against measured values of  $^3\text{He}$  determined by vacuum melting selected samples (7). The 10-15% differences in the values are most likely due to tritium off-gassing losses during storage and handling.

TABLE I Nominal Heat Compositions (wt%) and Mechanical Properties\*

Alloy	C**	Mn**	Si**	Cr	Ni	Mo	N	Other	Y.S. (MPa)	U.T.S. (MPa)
304L	0.03	2.00	1.00	19	10	-	-	-	483	931
316L	0.03	2.00	1.00	17	12	2.5	-	-	441	738
21-6-9	0.08	9.00	1.00	21	6	-	0.3	-	779	1138

\*All alloys were high energy rate forged

\*\*maximum.

The samples were pulled to failure at room temperature in air using a screw-driven testing machine and a crosshead speed of  $8.5 \times 10^{-3}$  mm/s. J-integral data were compiled from the load-displacement records using ASTM E 813-89 (8) and a crack estimation procedure developed by Hu, Albrecht, and Joyce (9). The J-integral for each load-displacement pair of the test record,  $J_{(i)}$ , was determined using the equations:

$$J_{(i)} = [K_{(i)}^2 (1-\nu^2) / E] + J_{pl (i)} \quad (1)$$

$$J_{pl (i)} = [\eta A_{pl (i)}] / [B b_{(i)}] \quad (2)$$

where  $K_{(i)}$  is the applied stress intensity (8);  $\nu$  and  $E$  are the material elastic constants;  $\eta$  is the plastic geometry factor (10);  $A_{pl (i)}$  is the area under the load-plastic displacement record;  $B$  is the specimen thickness; and  $b_{(i)}$  is the uncracked ligament. Crack initiation was assumed to be coincident with maximum load. The change in crack length prior to maximum load was assumed to be due to crack blunting and was calculated using the blunting line equations in ASTM E813-89 (8). Crack lengths after maximum load were estimated for each load-displacement pair by assuming that the change in compliance of the specimen was proportional to the measured load drop (9):

$$C_{(i)} = [P_{max} / P_{(i)}] C_0 \quad (3)$$

where  $C_{(i)}$  is the compliance at point  $i$ ,  $P_{max}$  is the maximum load,  $P_{(i)}$  is the load at point  $i$ , and  $C_0$  is the compliance calculated from measured values of the initial crack length. Crack lengths were calculated from the estimated compliance using the arc-specimen compliance equations given by Kapp and Bilinsky (11). The values of  $J$  at maximum load were assumed to be  $J_{Ic}$ ; these values are reported as  $J_Q$  values because the thickness of the specimens did not meet the requirements for plane strain (8). The reduced thickness was necessary in order to tritium charge the samples in reasonable times.

Helium bubble microstructures were characterized using transmission electron (TEM) microscopy. TEM disks were prepared from tritium-exposed Type 21-6-9 tensile bars that had been pulled to failure (6). Disks normal to the tensile axis were sliced from the grip (elastically strained) and the gauge sections (plastically strained) of each bar. These disks were then ground to  $\sim 0.1$  mm in thickness. Final thinning to produce electron transparent regions was performed using a twin-jet electropolisher using a potential of 11 V and the solution cooled to 258 K. The electrolyte consisted of 4 vol% HClO<sub>4</sub>, 40 vol % butylcellosolve, and 56 vol % methanol. After thinning, the foils were rinsed for about 60 seconds in a steady stream of ethanol. All specimens were examined in a Philips EM400T TEM operating at 120 kV.

### Results

For each of the alloys, tritium-exposed-and-aged samples had lower fracture-toughness ( $J_Q$ ) values and shallower sloped crack growth resistance (J-R) curves than control samples. This is shown in Figure 1 for Type 304L stainless steel. The  $J_Q$  values and the slopes of the J-R curves ( $dJ/da$ ) for all of the alloys as a function of the tritium and <sup>3</sup>He concentrations are listed in Table II. The 316L steel had higher overall fracture toughness values and more resistance to tritium-and-<sup>3</sup>He-induced reductions in fracture toughness values than the other steels. 21-6-9 stainless steel was embrittled the most. Moreover, the results show that increases in the <sup>3</sup>He content reduce further the  $J_Q$  and the  $dJ/da$  values, thus making crack initiation and

propagation even easier. The large decrease in the  $J_Q$  fracture-toughness value for the three alloys as a function of the surface (crack tip)  $^3\text{He}$  concentration is shown in Figure 2.

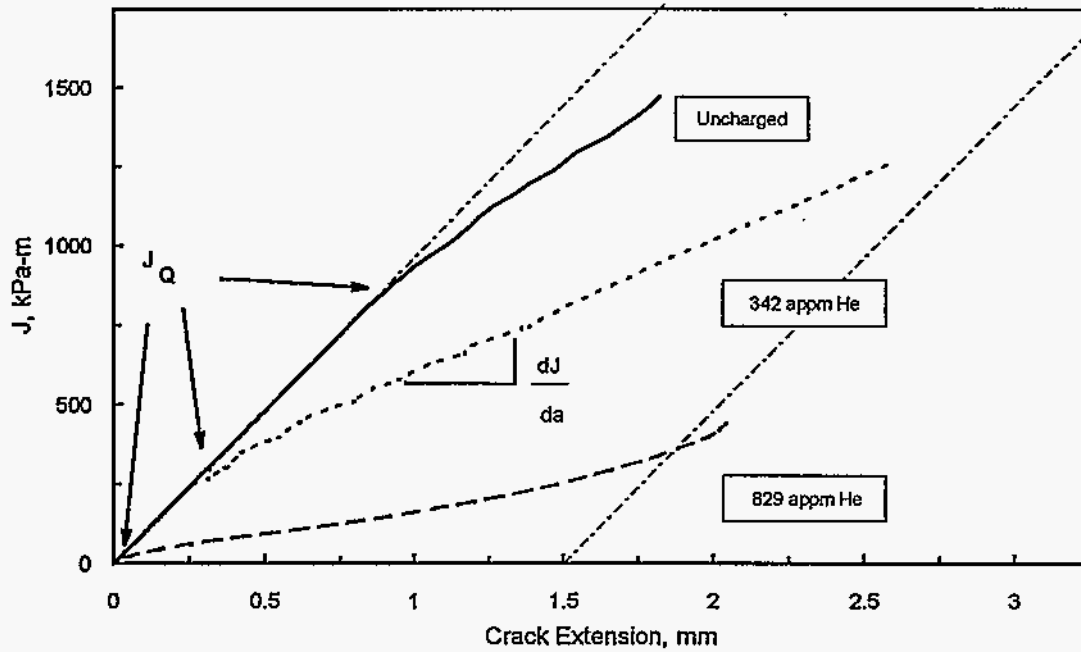


Figure 1. Effect of Increasing  $^3\text{He}$  Content on the J-R Curves of Tritium-Charged Type 304L Stainless Steel.

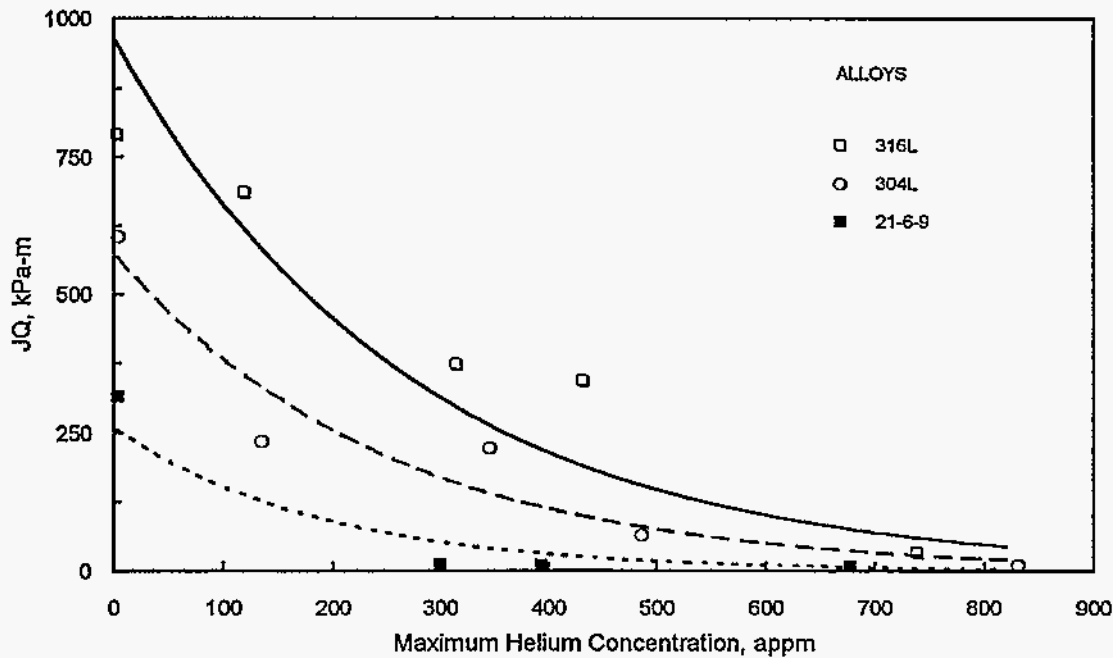


Figure 2. Fracture Toughness Reduction With Increasing  $^3\text{He}$  Concentration For Types 316L, 304L, And 21Cr-6Ni-9Mn Stainless Steels.

TABLE II Fracture Toughness Values

Alloy	Surface Concentrations (appm)			Fracture Toughness Values	
	Calculated T	<sup>3</sup> He	Measured <sup>3</sup> He	J <sub>Q</sub> * (kPa-m)	dJ / da* (MPa)
304L	0	0	---	608*	752*
	1522	131	116	241	521
	1253	342	---	230*	462*
	1093	483	---	71.5	221
	1430	829	---	18.7*	208*
	0**	342	---	751**	793**
316L	0	0	---	794*	917*
	1355	116	104	688*	827*
	1109	309	---	376*	683*
	978	425	---	349	516
	1272	737	---	39.0*	299*
21-6-9	0	0	---	320	717
	2606	296	246	18.2*	280*
	2497	390	---	16.1*	275*
	2165	674	---	15.6	167

\* average of duplicate samples

\*\* tritium degassed for 2 weeks @ 623 K

The fracture-toughness reductions were accompanied by a change in fracture mode from microvoid-nucleation-and-growth processes in uncharged samples to fracture along grain-and-twin boundaries in tritium-charged-and-aged samples. Figure 4a and 4b shows that increasing amounts of intergranular separation and twin-boundary parting occurred with increasing <sup>3</sup>He concentrations. The 316L stainless steel failed by primarily dimpled rupture even at <sup>3</sup>He levels as high as 309 appm (Figure 4c).

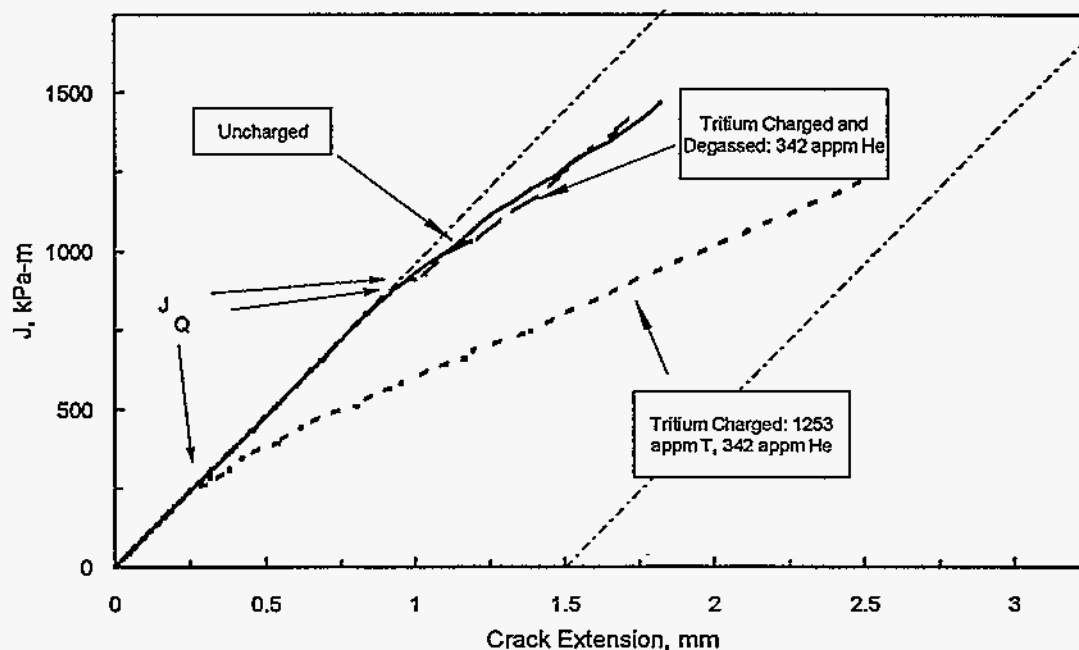
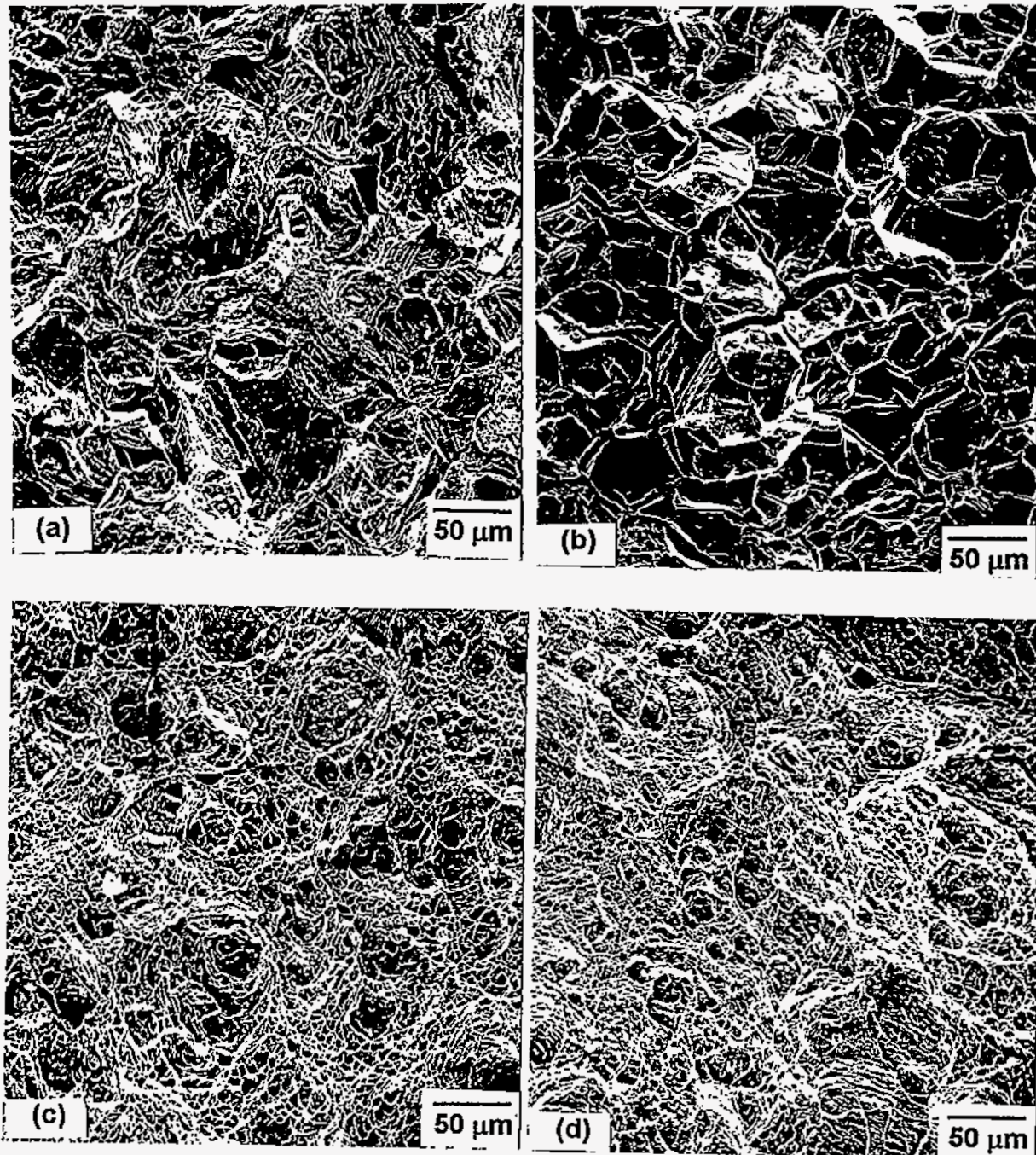


Figure 3. For Type 304L Steel Containing 342 Appm <sup>3</sup>He, Fracture Toughness Properties Were Restored Following Tritium Degassing.



The embrittling effects of tritium were separated from those of  $^3\text{He}$  by measuring the fracture toughness properties of tritium-charged-and-degassed samples of the 304L steel. Tritium degassing was performed by heating at 623 K for fourteen days. At this temperature, tritium is removed from the specimens while the  $^3\text{He}$  is trapped by lattice defects in the steel (2). For samples containing  $\sim 342$  appm  $^3\text{He}$ , the steel containing tritium and  $^3\text{He}$  had significantly reduced fracture toughness properties (Figure 3), while the tritium-degassed steel had fracture toughness properties and fracture modes that were similar to unexposed steels (Figure 4d).



**Figure 4.** Fracture Modes In Tritium-Exposed-And-Aged Stainless Steels: (a) Type 304L, 342 appm He; (b) Type 304L, 829 appm He; (c) Type 304L, Tritium Degassed,  $\sim 0$  appm T, 342 appm He (d) Type 316L Steel 309 appm He.

The microstructure of these steels was typical of HERF material and consisted of patches of ~ 5  $\mu\text{m}$  recrystallized grains embedded in much larger, ~ 200  $\mu\text{m}$ , unrecrystallized grains. The microstructure was approximately 15% recrystallized. The network of recrystallized grains indicates the onset of static recrystallization just after the final forging blow. Tritium-exposed-and-aged samples were characterized by the presence of  $^3\text{He}$  bubbles, whose strain fields give rise to the black dots within the recrystallized grains shown in Figure 5a. Although helium bubbles measuring between 1-2 nm were homogeneously distributed throughout the grain interiors, incoherent twin boundaries and dislocations were particularly potent nucleation sites. Figure 5b shows the large number density of bubbles associated with these defects. In recrystallized grains few dislocations were observed, but those that were present were "decorated" with a large number  $^3\text{He}$  bubbles.

Examination of specimens taken from the gage section (plastically strained) of tensile bars revealed differences in both  $^3\text{He}$  bubble microstructure and base microstructure when compared to the samples taken from the grips (elastically strained). In the plastically strained regions bubbles were readily observed on the high angle grain boundaries within the "patches" of recrystallized grains (Figure 5c). These bubbles measured approximately 2.0 nm in diameter and, in most instances, were present in large numbers. In many regions along the boundaries the bubbles appeared to have coalesced to form small cavities. Coalescence of bubbles was also observed at the incoherent twin boundaries. The bubble distribution within the matrix appeared to remain unchanged after deformation. The coalescence of bubbles on grain and twin boundaries following plastic deformation is consistent with the fracture modes shown in Figure 4.

The base microstructure following plastic deformation showed an increase in dislocation density as might be expected. However, the deformation modes exhibited within the "patches" of recrystallized grains were different than those within the unrecrystallized grains. Deformation occurred by intense planar slip within the recrystallized grains. In fact, in some cases cavities were observed at the intersection of dislocation pile-ups and grain boundaries. In the unrecrystallized, HERF grains deformation occurred by deformation twinning (Figure 5d).

In elastically strained regions,  $^3\text{He}$  bubbles were not observed on the high angle grain boundaries, i.e., those boundaries between recrystallized grains, HERF and recrystallized grains, or HERF grains. However, in one case strain contrast was observed along the boundary between two recrystallized grains. These observations and the fact that the fracture modes tended to be mostly intergranular suggests that bubbles are on the boundaries but, prior to plastic deformation, are smaller than the resolution limit of this imaging technique.

### Discussion

Tritium exposure made crack nucleation, as measured by JQ, and crack propagation, as measured by  $dJ / da$ , easier in each of these austenitic stainless steels. Furthermore, these fracture toughness properties decreased with increasing concentrations of  $^3\text{He}$  from tritium decay and were essentially restored on removal of the hydrogen isotopes from the steel. The type 316L stainless steel had the highest fracture toughness properties and the 21-6-9 steel the lowest. These results are in good agreement with those of earlier investigations by Robinson (1,2) and Caskey (12). In those studies, the fracture properties of both smooth and notched tritium-exposed-and-aged stainless steels decreased with increasing helium concentrations and tritium degassing caused a recovery of the fracture properties.



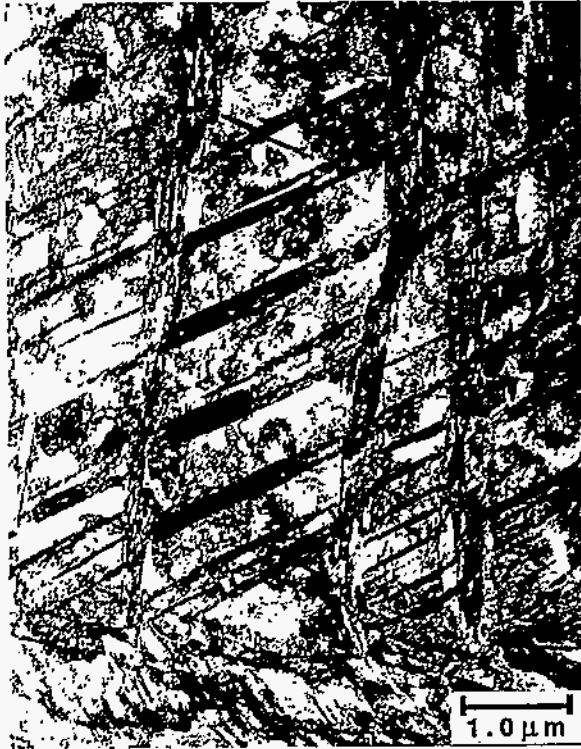
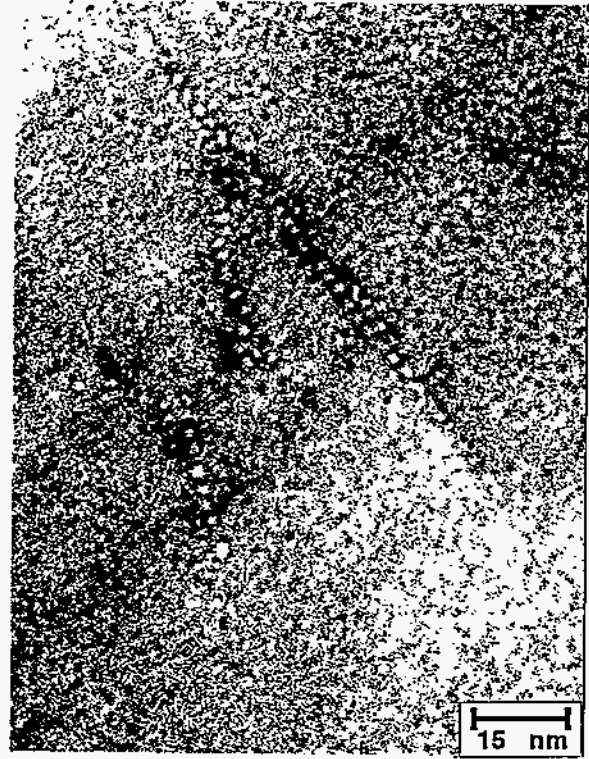


**Figure 5.** (a) Typical patch of recrystallized grains within the HERF microstructure. The strain fields associated with the helium bubbles give rise to the black dots in the recrystallized grain; (b) Helium bubbles associated with dislocations and an upright incoherent twin boundary; (c) Bubble growth and coalescence on a grain boundary; (d) Deformation twinning.

These fracture-toughness reductions and the relative ranking of the three steels are consistent with the predictions of the brittle fracture model of austenitic steels developed by Müllner, *et. al* (13). According to Müllner, brittle fracture will occur most easily in austenitic steels with low stacking fault energies and low densities of free dislocations. Steels with low stacking fault energies deform by twinning at lower strain levels than those with high stacking fault energies. Crack nucleation is made easier when twin lamella act as obstacles to further twin propagation. Twin lamella are effective obstacles when the density of free dislocations is low because the high stresses at the twin-twin intersections are not relaxed by dislocation motion.

In these tritium-exposed-and-aged steels, the density of free dislocations is reduced because of helium-bubble pinning. This changes the flow and fracture behavior in a number of ways. First of all, deformation twinning occurs more easily in steels containing helium from tritium decay (Figure 5d and Ref. 2). Secondly, crack nucleation is made easier because free dislocations are not available to relax the stress fields at twin-twin intersections and also because of the "cohesion lowering" effects of hydrogen when it is present in the lattice. Moreover, the strain field of the helium bubbles may enhance hydrogen embrittlement by trapping hydrogen at incoherent twin interfaces and grain boundaries which tend to be the typical sites for helium bubbles (Figure 5b,c) and the typical fracture paths (Figure 4). Abramov, *et. al* calculated the binding energy of hydrogen to helium bubbles to be approximately two or three times that of hydrogen to dislocations (15).

The relative toughness ranking of these alloys can be partly explained by their yield strength differences - fracture toughness tends to decrease with increasing yield strength. However, their relative susceptibility to tritium-induced embrittlement is consistent with the fracture model described above and earlier observations that showed increasing hydrogen embrittlement with decreasing stacking fault energy (16). The 21-6-9 steel had the lowest fracture toughness values and would be expected to have the lowest stacking fault energy because of its lower nickel (which tends to raise the stacking fault energy) content and its higher manganese and nitrogen (which tend to lower the stacking fault energy) contents. The fact that the 316L steel was less affected by tritium than the 304L steel could be explained by its higher nickel content.

### Conclusions

1. Tritium-exposed-and-aged steels had lower fracture-toughness values and less resistance to crack growth than unexposed steels. Fracture-toughness values were reduced further as the concentration of  $^3\text{He}$  increased from tritium decay.
2. In each of the tritium-charged steels the tendency toward intergranular fracture increased as the concentration of  $^3\text{He}$  from tritium decay increased.
3. Type 316L stainless steel was more resistant to the embrittling effects of tritium and  $^3\text{He}$  than the other steels. Type 21-6-9 was embrittled the most.
4. The fracture-toughness reductions are consistent with the "cohesion lowering" hydrogen embrittlement theories. Helium bubbles enhance hydrogen embrittlement by reducing the density of free dislocations, trapping hydrogen at grain boundaries, and making deformation twinning and crack nucleation easier.

## References

1. S. L. Robinson, *Materials Science. and Engineering*, 1987, vol. 96, pp 7-16.
2. S. L. Robinson, "The Effects of Tritium on the Flow and Fracture of Austenitic Stainless Steels", *Hyd. Eff. Mat'l Behavior*, N. R. Moody and A. W. Thompson, eds., TMS, Warrendale, PA, 1990, pp 433-445.
3. G. R. Caskey, "Hydrogen Effects in Stainless Steel", *Hyd. Degradation of Ferrous Alloys*, R. A. Oriani, J. P. Hirth, M. A. Smialowski, eds., Noyes Pub., 1985, pp 822-862.
4. M. J. Morgan, "The Effects of Hydrogen Isotopes and Helium on the Flow and Fracture Properties of 21-6-9 Stainless Steel", *Proc. Fine Symp.*, P. K. Liaw, J. R. Weertman, H. L. Marcus, and J. S. Santner, eds., TMS, Warrendale, PA, 1990, pp 105-111.
5. M. J. Morgan and D. Lohmeier, "Threshold Stress Intensities and Crack Growth Rates In Tritium-Exposed HERF Stainless Steels", *Hyd. Eff. on Mat'l Behavior*, N. R. Moody and A. W. Thompson, eds., TMS, Warrendale, PA, 1990, pp 459-468.
6. M. J. Morgan and M. H. Tosten, "Microstructure and Yield Strength Effects On Hydrogen and Tritium Induced Cracking In HERF Stainless Steels", *ibid*, pp 447-457.
7. B. M. Oliver, Rockwell International Report No. 86RC15250, 1986, Rockwell International, Rocketdyne Division, Canoga Park, CA.
8. ASTM E813-89, *Annual Book of ASTM Standards*, ASTM, Phila., PA, 1990, vol. 3.01.
9. Jun Ming Hu, Pedro Albrecht, and James A. Joyce, "Load Ratio Method for Estimating Crack Length", *Proc. of ASTM 22nd National Symposium on Fracture Mechanics*, 26-28, June 1990, Atlanta, GA.
10. E. Roos, *Trans. of ASME*, 1989, vol. 111, pp 252-258.
11. J. A. Kapp and W. J. Bilinsky, "J<sub>IC</sub> Testing Using Arc-Tension Specimens", *Frac. Mech.: Vol 17, ASTM STP 905*, J. H. Underwood, et. al, eds., ASTM, Phila, PA, 1986, pp 297-306.
12. G. R. Caskey, Jr., *Fusion Technology*, 1985, vol. 8, pp 2293-2298.
13. P. Müllner, C. Solenthaler, P. J. Uggowitzer and M. O. Speidel, *Acta metall. mater.*, 1994, vol. 42, No. 7, pp. 2211-2217.
14. J. C. M. Li, R. A. Oriani, and L. S. Darken, *Z. Phys. Chem.* 1972, vol.76, p. 848.
15. E. Abramov and D. Eliezer, "Synergistic Effects of Helium and Hydrogen Isotopes", *Hyd. Eff. on Mat'l Behavior*, N.R. Moody and A.W. Thompson, eds., TMS, Warrendale, PA, 1990, p. 169.
16. B. C. Odegard, J. A. Brooks, and A. J. West, "The Effects of Hydrogen on the Tensile Behavior of Nitrogen Strengthened Stainless Steel", *Eff. of Hyd. on Behavior of Mat'ls*, eds., A. W. Thompson and I. M. Bernstein (AIME 1977), 467-477.